

INFLUENCE OF INITIAL STATE AND HEAT TREATMENT CONDITIONS ON THE STRUCTURE OF RAPIDLY-QUENCHED TiNiCu ALLOY

A. A. Dyadechko^{1*}, I. A. Zaletova¹,
A. V. Shelyakov¹, N. N. Sitnikov¹,
and K. A. Borodako¹

Amorphous-crystalline alloy of the TiNi–TiCu quasi-binary system with 25 at.% copper content is prepared in the form of thin ribbons by rapid quenching from a liquid state. Completely amorphous ribbons are obtained using electrochemical polishing. It is shown that the crystal structure prepared by high-speed electropulsing heat treatment differ significantly from that prepared by isothermal heat treatment. The initial ribbon crystallizes as column-like crystals growing from both surfaces of the ribbon and as large lens-like crystals in the volume of the ribbon. The structure of column-like crystals reproduces the morphology and texture of the original crystalline layer. Reducing the electropulsing time to 1 ms increases the fraction of column-like crystals while their height increases and the width decreases. After the amorphous ribbon is crystallized, the structures of column-like crystals on both surfaces have similar crystallographic orientations.

DOI: 10.1134/S002247662104017X

Keywords: shape-memory alloys, amorphous state, crystallization, electropulsing heat treatment, crystal structure.

INTRODUCTION

The current state of science and technology makes great demands to novel materials, first of all to their multifunctionality. Such materials not only should possess unique physico-chemical properties but also demonstrate high operational characteristics. Shape-memory materials can meet all these requirements [1-3]. Copper-doped TiNi based alloys are bright representatives of this group of materials exhibiting unique properties [4-6]. The main feature of quasi-binary TiNi–TiCu alloys with a high copper content (more than 10 at.%) is that the hysteresis of martensitic transformation (MT) responsible for the shape-memory effect may be as small as a few degrees [7-12]. TiNiCu alloys obtained in the form of thin ribbons by rapid quenching from liquid state were shown prospective for the design of high-speed actuators in microelectromechanical systems (MEMS). In particular, rapidly-quenched alloy Ti₅₀Ni₂₅Cu₂₅ (at.%) [13-15] was effectively used in such microdevices (the B2 ↔ B19 MT hysteresis in this alloy is not more than 2-6 deg, while the value of its shape-memory effect is 3-8%, depending on the deformation method).

¹National Research Nuclear University MEPhI, Moscow, Russia; *kalba169@gmail.com. Original article submitted October 21, 2020; revised November 15, 2020; accepted November 23, 2020.

Note that amorphous TiNiCu alloys with high copper content (above 20 at.% Cu) can be obtained at high rates of melt cooling. Moreover, it was established that alloys crystallized from amorphous state possess better shape-memory characteristics [4, 6, 9]. There are various ways of crystal structure formation in an amorphous body, but one most promising is electropulsing heat treatment (EPT) whereby one or a series of electric current pulses are passed through the sample so that the material can crystallize without isothermal aging due to Joule heat release. In this case, EPT allows obtaining new structural states with unique properties.

This work is devoted to the study of the effect of electropulsing action on the formation and properties of the crystal structure in rapidly-quenched TiNiCu alloys depending on the initial state.

EXPERIMENTAL

Thin Ti₅₀Ni₂₅Cu₂₅ alloy ribbons were prepared by the melt spinning technique on the surface of a fast rotating copper wheel [4, 6]. The cooling rate varied in the range of 10⁵-10⁶ K/c. As a result, long ribbons with an average thickness of 28 μm and a width of about 1.5 mm were obtained.

The ribbons were crystallized by two methods: isothermally and by electropulsing. The isothermal heat treatment (ITT) was performed according to the standard technique in a muffle furnace at 500 °C with an aging time of 300 s and subsequent quenching in water. The crystallization by EPT was carried out by passing a single electric current pulse with a varying duration through the ribbon. For a fixed pulse duration, the amplitude of the current was chosen the way to ensure sufficient thermal energy release to heat the sample up to the crystallization temperature.

Electrochemical polishing (ECP) was performed using the thiourea-based electrolyte PLS/3 (Tekhnokom AS).

The structural parameters of obtained ribbons were studied using cross-sections made with the equipment for metallographic studies by Buehler company (Isomet 1000 precision cutter, Simplimet 1000 automatic hot mounting press, EcoMet 250+AutoMet 250 grinder and polisher machine). The microstructure of the samples was studied using a Carl Zeiss Axiovert 40 MAT inverted reflected-light metallographic microscope and a FEI Quanta 600 FEG scanning electronic microscope (SEM). For better visibility, the polished surface was etched with a HF (5%) + H₂NO₃ (25%) + H₂O (70%) solution for 10-30 s and then wiped with a 3% H₂O₂ solution to remove the remaining etching products.

The X-ray diffraction analysis was carried out on PANalytical Empyrean and Shimadzu XRD-6000 diffractometers using CuK_α radiation. Thin structure of alloys was studied by a JEOL JEM 2100 high-resolution transmission electron microscope (TEM).

RESULTS AND DISCUSSION

As a result of X-ray studies of the Ti₅₀Ni₂₅Cu₂₅ alloy, XRD patterns were obtained for contacting (facing the quenching wheel) and free (non-contacting) surfaces of the ribbon. The structural differences between these patterns can be seen in Fig. 1. The XRD pattern of the contacting surface in the initial state has a broad diffuse maximum (halo) without any structural peaks. To the contrary, the pattern of the free surface exhibits pronounced diffraction peaks of both the martensite phase **B19** (orthorhombic martensite) and the austenite phase **B2** (CsCl type bcc lattice) as well as a sign of amorphous halo indicating small thickness of the crystal layer.

The SEM study of ribbon cross-sections revealed a sharp boundary between amorphous and crystal layers without a noticeable transition region and showed that the crystal layer has a column-like structure (Fig. 2a). It was established that the ribbons have a layered structure with an average amorphous layer thickness of 25.5 μm and an average crystal layer thickness of 2.5 μm.

The TEM study of the crystal layer structure showed that a plate-like structure (characteristic of martensite) with an average plate size of 30-80 nm appears in the grains of the crystal layer at room temperature and that the microdiffraction pattern of this region corresponds to orthorhombic martensite **B19** (Fig. 3a). The TEM images of the contacting surface

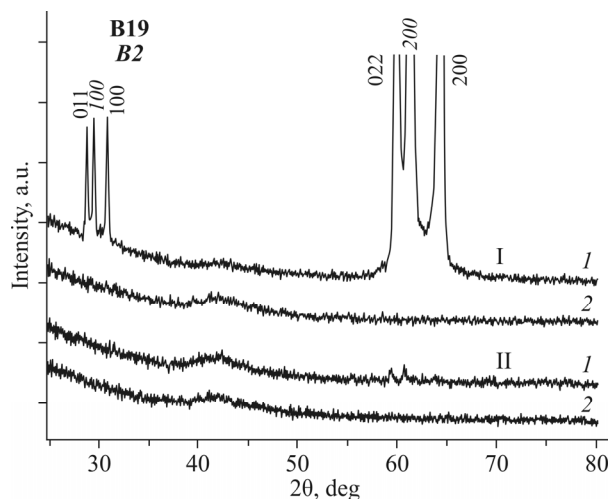


Fig. 1. XRD patterns of the rapidly-quenched ribbon obtained from the $\text{Ti}_{50}\text{Ni}_{25}\text{Cu}_{25}$ alloy in the initial state (I) and after electrochemical polishing (II) recorded from the free (1) and the contacting (2) surface (**B19** is the AuCd type martensite phase, **B2** is the CsCl type austenite phase).

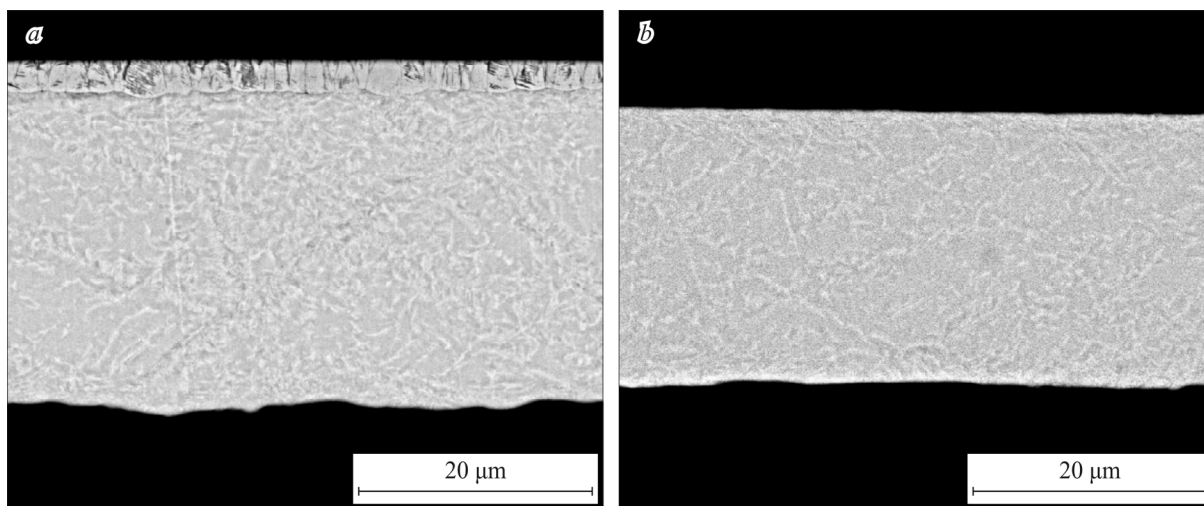


Fig. 2. Cross-section SEM images of the rapidly-quenched ribbon of the $\text{Ti}_{50}\text{Ni}_{25}\text{Cu}_{25}$ alloy before (a) and after (b) removing the crystal layer.

(Fig. 3b) show an ultradispersed absorption contrast typical of amorphous phases, while the corresponding electron diffraction pattern exhibits a number of diffuse rings with decreasing intensities as the diffraction angle increases.

The obtained data suggest that the ribbon in the initial state after quenching is an amorphous-crystalline composite with a sharp homogeneous boundary between the layers. To prepare a completely amorphous ribbon, the surface crystalline layer was removed by electrochemical polishing (ECP) for 12 min at a voltage of 5 V. Complete removal of the crystalline layer was ensured by using cross-sections of the studied ribbon. The cross-section image of the ribbon after ECP shows no presence of the crystalline layer, the average thickness of the amorphous ribbon is 22 μm , and the ribbon has quite a uniform shape throughout the cross-section (Fig. 2b). According to the XRD data obtained for contacting and free ribbon surfaces after ECP (Fig. 1), the XRD patterns of the contacting surface contains no structural peaks while those of the free surface contain low-intensity peaks of the martensite phase due to the presence of individual crystals inside the amorphous matrix.

Crystallizing the ribbon in the initial state showed that ITT leads to the formation of bimorphic crystal structures consisting of a recrystallized crystalline layer (from the free surface) and a crystal layer formed from the amorphous part of

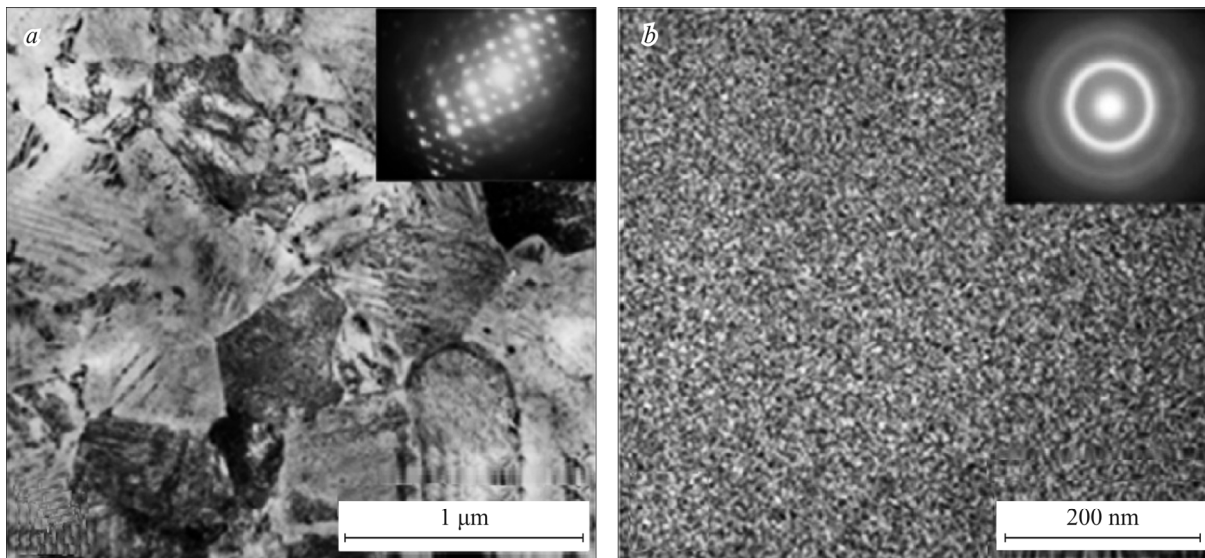


Fig. 3. TEM images of crystalline (*a*) and amorphous (*b*) layers and the corresponding electron diffraction patterns.

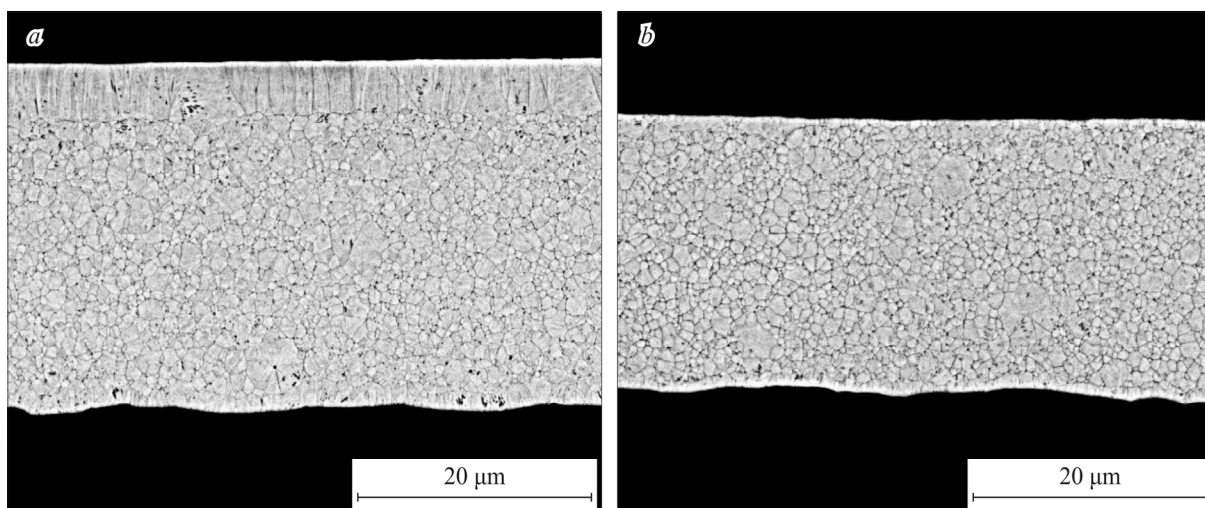


Fig. 4. Cross-section microstructure of the isothermally crystallized ribbon in the initial state (*a*) and after electrochemical polishing (*b*).

the ribbon (Fig. 4*a*). The layer from the free surface preserves the column-like structure which is mainly uniform in thickness (5-6 μm), while the boundary with the crystals formed from the inner part of the ribbon is smooth and distinct. Note that the average thickness of the initial crystalline layer surface was 2.5 μm to testify its growth during the heat treatment. The crystalline layer formed from the amorphous part on the contacting surface exhibits a uniform submicron structure.

The sample that was isothermally heat-treated after ECP shows almost no surface column-like crystals, while the crystal structure in general shows a uniform distribution of submicron crystals (Fig. 4*b*). The surface contains local areas with column-like crystals which might be formed either due to the incompletely removed initial crystalline layer or due to the fact that the free surface still preserved some textured or defect structure.

EPT treatment significantly changes the nature of crystal formation in the amorphous ribbon compared to ITT treatment (Fig. 5). The cross-section structure of the ribbon shows an inhomogeneous distribution of crystals: column-like crystals occur near the surfaces of the ribbon while the volume of the ribbon contains individual or grouped large crystals. Under the action of electric current for 5000 ms, the column-like crystals on both surfaces of the ribbon grow inside at

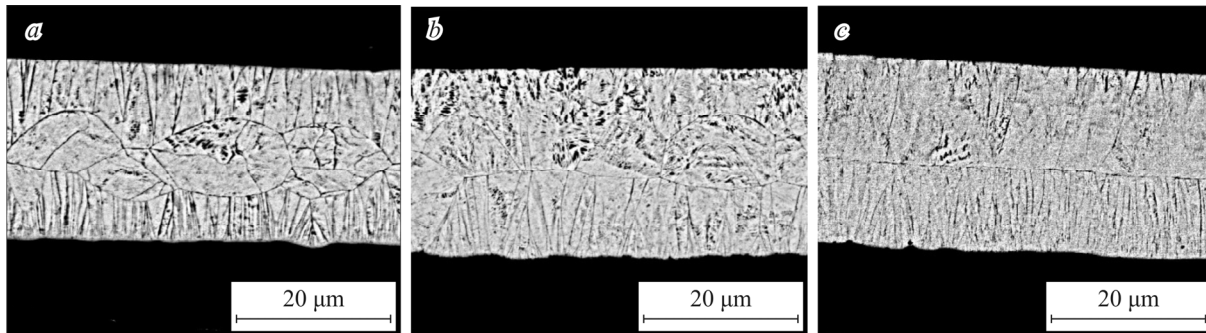


Fig. 5. Microstructure of the ribbon cross-section after EPT treatment for 5000 ms (*a*), 10 ms (*b*), 1 ms (*c*).

different depths to form an uneven boundary with the crystals from the inner region (Fig. 5*a*). At the same time, the height and width of the column-like crystals are somewhat larger from the free surface of the ribbon than from the contacting surface.

As the pulse duration decreases to 10 ms, the rate of crystals growth from the surface begins to exceed the rate of crystals formation in the inner part of the ribbon. Thus, we conclude that decreasing the EPT duration increases the fraction of column-like crystals formed on the ribbon surfaces from the amorphous part and makes them thinner, whereas the fraction of crystals formed in the inner part decreases and their shape (in the case of individual crystals) becomes lens-like (Fig. 5*b*). Also, there are areas containing no inner crystals and exhibiting a distinct boundary (Fig. 5*c*).

The obtained XRD data confirmed that IHT and EPT cause crystallization of the amorphous state to form orthorhombic martensite **B19** (Fig. 6), while EPT (in contrast to ITT) causes no radical changes in the positions of crystallographic reflections. The XRD patterns of the free surface show reflections uncharacteristic of phase **B19**: the peaks of highest intensity and area occur in the 58–65° region, whereas smaller peaks occur in the 39–45° region (Fig. 6*a*). This means that the “texturing effect” from the initial surface crystal layer is still preserved after thermal treatment. At the same time, the main crystallographic reflections on the XRD patterns of the contacting surface occur in the 39–45° region (Fig. 6*b*), which is typical of the **B19** phase and corresponds to their position after ITT. Note that the intensity of the peaks from the contacting surface is smaller than that from the free surface.

The obtained data suggest that structures with different crystallographic orientations are formed from different surfaces of the ribbon as a result of EPT treatment. This phenomenon may be due to the influence of incompletely removed initial surface crystalline layer or due to residual strains at its boundary with the amorphous part. It was established that the column-like crystals formed as a result of EPT and growing from the free surface from the residues of the initial crystalline

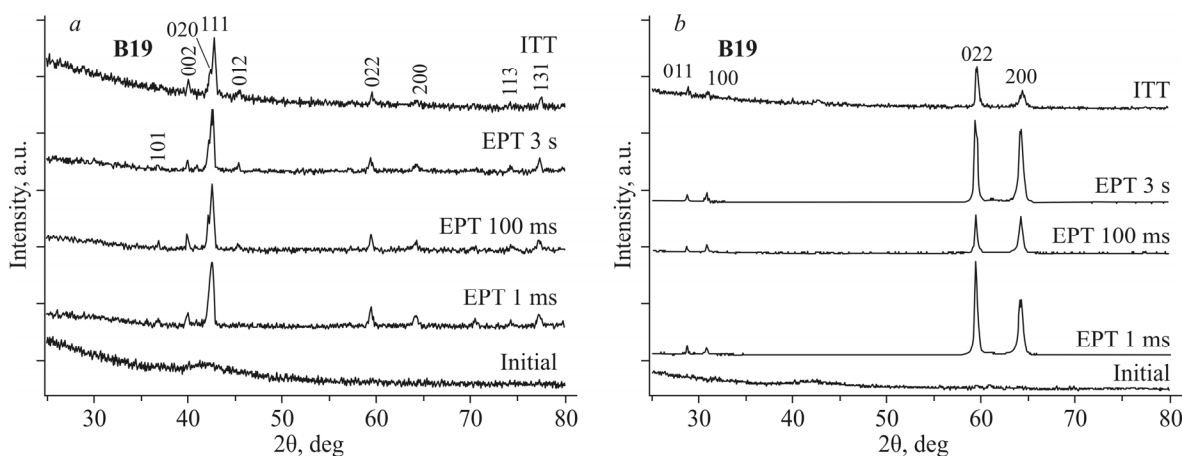


Fig. 6. XRD patterns of contacting (*a*) and free (*b*) surfaces of the ribbon in the initial state and after heat treatment: isothermal (ITT) and electropulsing (EPT) of different durations (1 ms, 100 ms, 3 s).

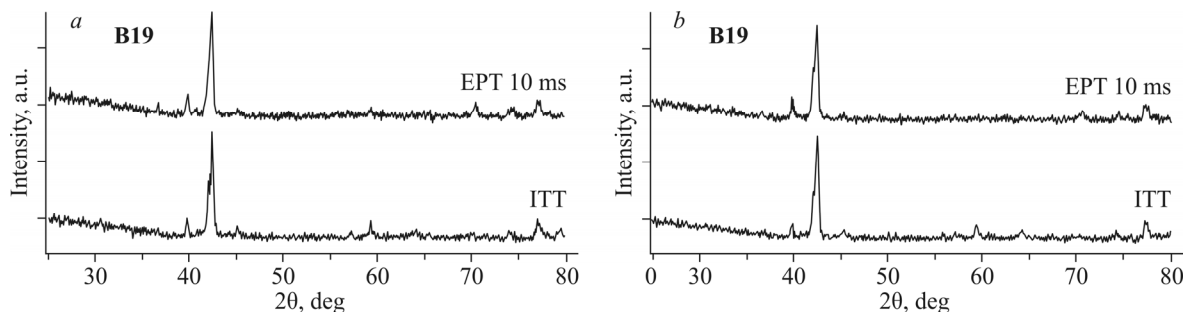


Fig. 7. XRD patterns of contacting (*a*) and free (*b*) surfaces of the ribbon after ECP for 20 min and subsequent crystallization heat treatment: isothermal (ITT) and electropulsing (EPT) for 10 ms.

layer or from crystalline inclusions on the surface of the rapidly-quenched ribbon reproduce its structural morphology and texture. Therefore, we prepared an additional series of ribbons subjected to ECP treatment for 20 min, standard ITT treatment, and EPT treatment for 10 ms. The X-ray analysis of the samples from free and contacting surfaces showed that the peak positions in the XRD patterns of these samples have identical locations while their reflections of phase **B19** have comparable intensities (Fig. 7).

The XRD patterns of the free surface of the ribbon contain no peaks that would reproduce the structural morphology and texture of the initial surface crystalline layer. The obtained data suggest that a structure of column-like crystals with the same crystallographic orientation is formed in the direction from both surfaces as the initial surface layer is completely removed by ECP.

CONCLUSIONS

An alloy of the quasi-binary system TiNi–TiCu with the a copper content of 25 at.% was prepared by rapid quenching from the melt in the form of a layered amorphous-crystalline ribbon. Novel structural states were obtained by electropulsing heat treatment in the alloy. EPT treatment with a duration of less than 5 s significantly changes the resulting crystal structure compared with that obtained by standard isothermal heat treatment for 300 s at 500 °C.

- After EPT, the cross-section microstructure of alloys shows an inhomogeneous distribution of crystals over the ribbon thickness: a structure of column-like crystals is formed near the surfaces while the volume contains individual or grouped large crystals. The observed column-like crystals grow from the surface inside the ribbon to the crystals formed in its volume, while some part of the column-like crystals contact each other in the center of the ribbon to form a uniform boundary.

- Decreasing the duration of electropulsing action to 1 ms increases the fraction of column-like crystals, while their height increases and the width decreases.

- The column-like crystals growing from the free surface of the ribbon from the initial surface crystal layer reproduce the structural morphology and texture of the latter.

- As the surface crystalline layer is completely removed by electrochemical polishing, a structure of column-like crystals having equal crystallographic orientations is formed from both surfaces of the ribbon during EPT.

FUNDING

The study was funded by Russian Science Foundation (project No. 19-12-00327).

CONFLICT OF INTERESTS

The authors declare that they have no conflict of interests.

REFERENCES

1. M. Kohl, H. Ossmer, M. Gueltig, and C. Megnin. *Shape Mem. Superelasticity*, **2018**, 4, 127.
2. K. Otsuka and X. Ren. *Prog. Mater. Sci.*, **2005**, 50, 511.
3. J. M. Jani, M. Leary, A. Subic, and M. A. Gibson. *Mater. Des.*, **2014**, 56, 1078.
4. A. V. Shelyakov, N. N. Sitnikov, A. P. Menushenkov, A. A. Korneev, R. N. Rizakhanov, and N. A. Sokolova. *J. Alloys Compd.*, **2013**, 577, S251.
5. A. Ishida, M. Sato, and Z. Y. Gao. *J. Alloys Compd.*, **2013**, 577, S184.
6. A. V. Shelyakov, N. N. Sitnikov, A. P. Menushenkov, V. V. Koledov, and A. I. Irjak. *Thin Solid Films*, **2011**, 519, 5314.
7. S. W. Kang, Y. M. Lim, Y. H. Lee, H. J. Moon, J. W. Kim, and T. H. Nam. *Scr. Mater.*, **2010**, 62, 71.
8. P. Schlossmacher, N. Boucharat, G. Wilde, H. Roesner, and A. V. Shelyakov. *J. Phys. IV France*, **2003**, 112, 731.
9. B. V. Senkovskiy, D. Yu. Usachov, A. V. Fedorov, O. Yu. Vilkov, A. V. Shelyakov, and V. K. Adamchuk. *J. Alloys Compd.*, **2012**, 537, 190.
10. S. H. Chang, S. K. Wu, and H. Kimura. *Intermetallics*, **2007**, 15, 233.
11. Y. X. Tong, Y. Liu, and Z. L. Xie. *J. Alloys Compd.*, **2008**, 456, 170.
12. C. H. Chen, H. K. Wang, and S. K. Wu. *Intermetallics*, **2018**, 93, 347.
13. A. Shelyakov, N. Sitnikov, K. Borodako, V. Koledov, I. Khabibullina, and S. Gratowski. *J. Micro-Bio Rob.*, **2020**, 16, 43.
14. A. V. Shelyakov, N. N. Sitnikov, V. V. Koledov, D. S. Kuchin, A. I. Irzhak, and N. Yu. Tabachkova. *Int. J. Smart Nano Mater.*, **2011**, 2(2), 68.
15. A. Shelyakov, D. Rozhkov, N. Sitnikov, A. Menushenkov, A. Timofeev, and M. Berezin. *Mater. Today: Proc.*, **2017**, 4, 4870.